Fifth International Conference on CFD in the Process Industries
CSIRO, Melbourne, Australia
13-15 December 2006

A CFD MODEL OF A SUBMERGED ARC FURNACE FOR PHOSPHOROUS PRODUCTION

Emile SCHEEPERS[1], Allert T. ADEMA[1], Yongxiang YANG[1], Rob BOOM[1] and Markus A. REUTER[2]

[1] Material Science and Engineering, Delft University of Technology, THE NETHERLANDS
[2] Department of Chemical and Biomolecular Engineering, The University of Melbourne, AUSTRALIA

ABSTRACT

Within the packed bed of a phosphorous producing, submerged arc furnace, solid-gas reactions are dominant in generating the gaseous product. These reactions are the main focus in the development of a quantitative CFD model. The associated process complexities necessitated the creation of process-specific, user-developed models that integrate accurate, multi-field thermodynamical data with computational flow dynamic calculations and kinetics: The Reaction model accounts for the downward flow and reduction of P_2O_5 as a function of reaction kinetics and temperature, the subsequent creation of P_4 and CO from within the packed bed domain as well as the energy sinks due to heating, reaction and melting. Thermal radiation modelling within the packed bed is improved by subliment modelled with the help of a user-developed particle-particle radiation model. The results provide fully, three-dimensional furnace characteristics of gas flow, energy distribution and chemical reactions. This CFD model forms part of a larger project that aims to create a Dynamic-CFD hybrid control model.

NOMENCLATURE

k	thermal conductivity [W/m.K]
k_{eff}	effective thermal conductivity [W/m.K]
ρ	density [kg/m^3]
ρ_{pb}	density of the packed bed [kg/m^3]
T	temperature [K]
a	absorption coefficient
s	scattering coefficient
Q_{HM}	Energy sink due to heating and melting [W/m^3]
Cp	Specific heat capacity [J/kg·K]
ΔT_z	Temperature gradient in the downward direction [K/m]
W	Downward packed burden velocity [m/s]

INTRODUCTION

The process under investigation is the large-scale production of phosphorus at Thermphos, The Netherlands. The main reaction as defined by the Wöhler process (Corbridge 1995), proceeds according to Equation 1, producing a calcium-silicate slag, calcium fluoride, carbon monoxide and the desired product, phosphorus gas.

$$Ca_{10}\left(PO_4\right)_6 F_2 + 15C + 9SiO_2 \rightarrow 3P_{2(g)} + 9\left[\left(CaO \cdot SiO_2\right)\right] + CaF_2 + 15CO_{(g)} \quad (1)$$

Gravity delivers the feed, consisting of apatite, coke and silica, to the furnace through ten, evenly distributed feed chutes ensuring constant packed bed volume. The gaseous product leaves the furnace through two symmetrically spaced outlet vents situated above the ferrophosphorous tap hole in the roof of the furnace. The ferrophosphorous is tapped off, usually once per day. Slag, however, is continuously tapped through two alternating, water-cooled tapping holes located 400 mm above the furnace floor (see Figure 1). Owing to the large production volume of slag, a seemingly small amount of P_2O_5 in the slag results in substantial losses of unreduced, potential product. Controlling the process in order to keep the P_2O_5 wt% in the slag as low as possible is therefore one of the top priority at Thermphos. Their efforts are being assisted through the creation of a Dynamic-CFD hybrid control model for the submerged arc furnace. Scheepers, Yang, Adema and Reuter (2006) describes in detail how a standard linear transfer function model (Auto Regressive Exogenous - ARX), utilising intelligently structured data, can have powerful predictive abilities and provide online decision support. It also sets out the initial construction work of a CFD model. Scheepers, Adema, Yang & Reuter (2006) describes in detail the development of two user-developed, process-specific models, a unique way of constructing Derived-CFD variables in order provide additional decision support for the Dynamic-CFD hybrid model as well as preliminary results. This paper is the continuation of that work and will discuss the following:

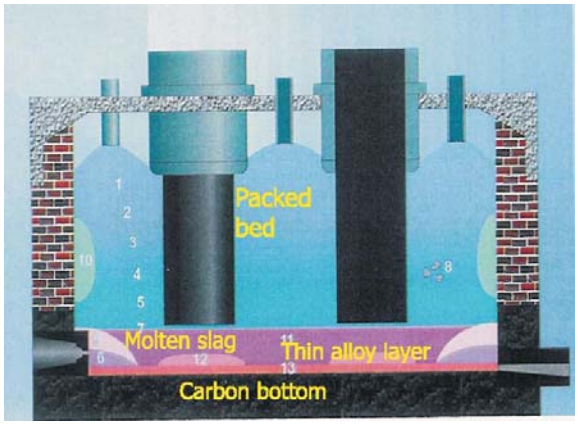

Figure 1: A cut-through graphical depiction of a submerged arc furnace. (Dresen et al. 2002).

- The dimensions, structure and computational grid of the constructed submerged arc furnace, the input - and boundary conditions as well as a review of the standard models utilised

- A short summary of the two user-developed, process-specific models
- An in-depth discussion of the most up-to-date solved model and a sensitivity analysis review by looking at four previously solved models
- Model validation techniques and concluding remarks

The creation of this CFD model also addresses another top priority - the understanding and eventual minimisation of the varying energy consumption created by complex mixtures of primary and as well as secondary, recycled, phosphorus containing feed materials. By generating a virtual window to the inside of the furnace, operators can get an idea of the changing conditions inside the furnace as a result of changing feed materials.

CFD-BASED PROCESS MODEL

Work by Dresen et al. (2002) and Van der Pas (1999) revealed that the solid-gas reactions inside the packed bed itself are responsible for most of the production of the gaseous product. It is also inside the packed bed region where the rate-limiting steps of the process are located. It is for these reasons that the packed bed region inside the furnace is the focus of the modelling.

General information of the CFD-model

For this study a general purpose, CFD code Fluent 6.1.18 (2003) was used. Fluent 6.1.18 (2003) has standard models to solve most of the required governing equations. The standard physical models used included the standard k-ε turbulence model and P1 radiation model. Multiple simulations showed that more complex models did not provide any significant improvements. The Fluent 6.1.18 (2003) Porous Media Model was used for the packed bed area, where the particles had an average diameter of 2cm. The complexities associated with the production of phosphorous, however, necessitated the creation of process specific models. These user-developed models were coded in C++, coupled to Fluent 6.1.18 (2003) and solved exactly the same way as the above-mentioned standard models.

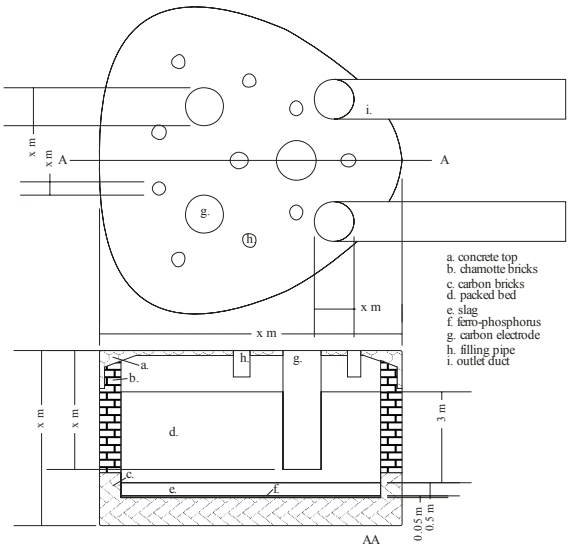

Figure 2: Some selected dimensions of the furnace utilised in the CFD model. Owing to confidentiality agreements, some dimensions are not mentioned

These user-developed models include a Reaction model and a Particle-particle radiation and effective thermal conductivity model. These two models are reviewed later.

Furnace dimensions, structure and computational grid

The furnace model to be used in Fluent 6.1.18 (2003) was constructed and meshed in Gambit 2.04 (2003) using the dimensions as seen in Figure 2. The furnace has a carbon brick bottom lining, chamotte brick side lining and a concrete top with three amorphous, carbon electrodes. A hexagonal mesh scheme (Cooper type) was used for the furnace and both a tetrahedral/hybrid mesh scheme (T-grid type) and hexagonal mesh scheme were used for the outlet ducts. The total number of cells is 414000 and typical solving times were between 12 - 20 hours. The entire body of the furnace lining was constructed as a conducting solid using the individual manufacturer specifications of each type of lining but the formation of freeze-lining had not been taken into consideration at the time of publications. The electrodes were modelled with actual property values and the outlet duct has a zero thickness and was abnormally extended in order to establish fully developed flow and at the same time minimise the effect of reversed flow - a phenomenon often encountered in CFD modelling. The packed bed inside the furnace is represented with the Fluent 6.1.18 (2003) porous media model, as well as with two above-mentioned user-developed models. Below the packed bed, the slag and ferrophosphorous phases are simplified as non-flowing, liquid layers but still retain all material properties associated with the respective phases. Although modelling results are presented in a two-dimensional way in the Results section, the furnace model is entirely three-dimensional and all standard-and user-developed models are solved three-dimensionally.

Input and boundary conditions

Energy input (Arcs)

Gu & Irons (1998) employed a channel arc model that showed how the arc from an electrode could by approximated by a cylinder. For this reason, three cylindrical inlet volumes were created between the electrode tips and the slag surface while the diameter of the electrodes was used as the diameter of the inlet volumes. The power supplied by the three electrode arcs is introduced as constant, positive heat fluxes to the model through these inlet volumes underneath the electrodes. Theoretically, for an industrial phosphorus furnace, the energy is distributed between heating up and melting of the material (≈ 31%) and chemical reactions (≈ 53%) (Robiette & Allen 1972) (Ullmann's Encyclopedia of Industrial Chemistry 2000). Cooling losses account for the additional energy (≈ 16%). One of the aims of this study was to investigate this distribution ratio (see results Table 2a,b).

Cooling water

In the model, the actual, convective losses experienced at Thermphos were simulated in the model by introducing averaged, negative heat fluxes over the bottom cooling, side cooling and electrode cooling surfaces.

Exposed furnace surface

In the model, radiative heat losses were compensated for by introducing a mixed boundary regime across the relevant surface that included radiation and convective heat losses. The parameters were radiation ambient temperature = 623K, emissivity = 0.8 for oxidised steel (Incropera and De Witt

1990), convection ambient temperature = 573K and convection coefficient = 10[W/m^{2}K].

User-developed models

Reaction Model

The energy introduced to the model through the inlet zones is distributed between the energy required for heating up and melting of the packed bed material and the energy required for the gaseous product formation (simplified to Equation 2). This distribution was facilitated through the creation of a Reaction model that incorporates these phenomena by integrating fundamental thermodynamics with kinetic data. The following is created and accounted for in the Reaction model:

Creation P_2O_5 concentration in the packed bed: A user-developed scalar value representing the concentration of unreduced P_2O_5 in the pellets ($P_2O_5^S$) was created in the model [kg/m^3]. The initialisation value for this scalar of 229 [kg P_2O_5 /m^3] used in this paper corresponds to a 29.1wt% P_2O_5 in the pellets and a packed bed porosity of 37.7%. This initialisation value is a function of the type of apatite ore Thermphos International was using at the time of modelling.

Creation of virtual, downward-velocity of the packed bed: Downward burden movement is simulated through the creation of a virtual, user-developed flux [1/s] perpendicular to the furnace floor. By means of this packed bed flux, the user-developed scalar value ($P_2O_5^S$) is transposed downward through the packed bed domain at the rate of descent of the actual packed bed. This parameter is referred to as $P_2O_5^F$ [kg/m^3.s].

Reaction kinetics, P_2O_5 consumption and gaseous product creation: Throughout the iterative solving process of the model, the unreduced P_2O_5 [kg/m^3] left in the pellets ($P_2O_5^F$ [New]) is used to calculate the rate of change of P_2O_5 concentration in the packed bed ($\Delta P_2O_5^F$) as the reaction takes place. For these calculations a simplified version of Equation 1 was utilised. The overall simplified reaction is depicted in Equation 2.

$$2Ca_3\left(PO_4\right)_2 + 10C + 6SiO_2 \rightarrow P_{4(g)} + 6CaSiO_3 + 10CO_{(g)} \quad (2)$$

The onset temperature of ≈1150°C for P_2O_5 reduction was determined experimentally and the reaction is also assumed to take place in two specific steps (Dresen, 2002): Equation 3 is the liberation step and Equation 4 the diffusion step.

$$Ca_3\left(PO_4\right)_2 + 3SiO_2 \rightarrow 3CaSiO_3 + P_2O_{5(gas)} \quad (3)$$

$$P_2O_{5(gas)} + 10C \rightarrow P_{4(gas)} + 10CO_{(gas)} \quad (4)$$

Equation 2 is a first order reaction, reacting according to a shrinking core model (Mu, 1986). In the shrinking core model the P_2O_5 gas in Equation 3 is liberated from a reaction surface moving from the outside to the inside of the pellet and is controlled by the removal rate of gases from the reaction surface. The reaction constants for a variety of apatite feed ores are calculated from empirical equations obtained experimentally through kinetic investigation of actual feed sample provided by Thermphos International (Van der Pas, 1999). Equation 4 shows the experimentally determined reaction constant equation for the specific ore of which the results are presented in the paper.

$$k = 2.58 \times 10^{-4} \cdot T - 0.3795 \quad (5)$$

The rate of change of the P_2O_5 as a result of Equation 2 to 4 is now calculated through the following derived Equation 6, where t = 1 second and k is the reaction constant of Equation 5.

$$\Delta P_2O_5^F = -k \cdot P_2O_{5[Old]}^F \cdot e^{-kt} \cdot \left[\frac{1}{60}\right] \quad (6)$$

The remaining amount of P_2O_5 ($P_2O_5^F$ [New]) is then given by Equation 7.

$$P_2O_{5[New]}^F = P_2O_{5[Old]}^F + \Delta P_2O_5^F \quad (7)$$

Equation 8 initialises a new P_2O_5 value for the next iteration (Equation 6 once again) in the solving algorithm of the CFD model.

$$P_2O_{5[Old]}^F = P_2O_{5[New]}^F \quad (8)$$

Equations 6 to 8 are embedded in a coded loop structure within the model.

$\Delta P_2O_5^F$ is the amount of P_2O_5 that reacts according to Equation 2 every second [kg/m$_3$·s]. This rate of P_2O_5 decrease in the packed bed is used to determine the volumetric mass generation rate of the gaseous products. From theory it is determined that each kilogram of P_2O_5 produces 0.44 kg of P_4 and 1 kg of CO gas. The amount of P_4 and CO generated is then introduced into the model. The amount of P_4 and CO generated is also used in the determination of the energy distribution within the packed bed.

Energy sink due to Reaction (Gaseous product): All individual component feed streams at Thermphos were recalculated on the basis of an input of 1kg of P_2O_5 per second and solved in Factsage. The equilibrium energy needed as a result of gaseous product formation and phase transformation is calculated as a function of temperature and depicted in Figure 3.

The twelve values indicated in boldface are used to construct a trend line from which the energy required for gaseous product formation at a specific temperature can be obtained. These values are then multiplied with the loss of P_2O_5 value ($\Delta P_2O_5^F$) within each individual cell contained in the packed bed reactor domain in order to obtain the total energy sink to be employed over the same domain [W/m^3].

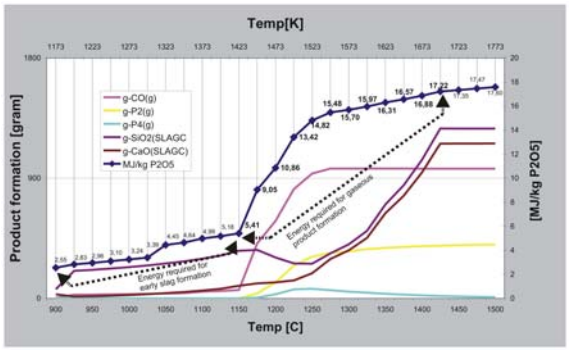

Figure 3: The energy required for early slag formation, the energy required for subsequent gaseous product and slag formation, as well as the theoretic amount of product (given an initial amount of 1kg P_2O_5) formed.

Energy sink due to Reaction II (Early slag formation): Although no gaseous product is formed below ≈ 1150°C, slag formation below this temperature consumes energy. Figure 3 also depicts the energy required for this phenomenon. It is, however, not possible here to mathematically connect the overall energy required to the loss of P_2O_5 value because below 1150°C it has not started yet.

Energy sink due to heating and melting: By using individual component feed stream data, the overall heat capacity (Cp) value for the packed bed was calculated for temperatures between 373K and 3373K. The raw Cp data, as well as corresponding trend lines, are presented in Figure 4.

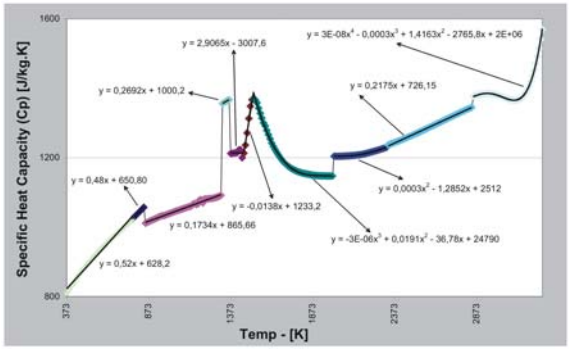

Figure 4: The heat capacity values for the packed bed over a temperature range.

With temperature dependent Cp values available, an energy sink as a result of heating and melting is employed over each individual cell in the packed bed domain through the use of Equation 9 within the coded structure of the model. The energy required to heat and melt the feed is therefore immediately compensated for.

$$Q_{HM} = -Cp \cdot \rho_{pb} \cdot \Delta T_{Z[cell]} \cdot W \quad (9)$$

Particle-particle radiation and effective thermal conductivity model

The porous media model calculates the thermal conductivity by taking a volumetric average based on the porosity of the packed bed. Thermal radiation between particles is not taken into account while at high temperatures in the furnace this is a very important way of heat transfer. In order to therefore improve the standard porous media model for high temperatures, the two conductivity values for the solid (furnace feed) and of the fluid (gaseous product) were replaced by a single, temperature-dependent effective thermal conductivity value representing actual furnace conditions more accurately. The result was an effective thermal conductivity value (k_{eff}) to be used in Fluent6.1.18 (2003) that incorporated both conductive, as well as particle-particle radiative aspects based on actual process conditions. The gas radiation within and above the packed bed is computed by the standard P1 radiation model. The mathematical development of this user-defined model can be found in Scheepers, Adema, Yang & Reuter (2006).

Cokes conductivity and Joule heating of the electrodes

In order to compensate for cokes conductivity as well as arc radiation, k_{eff} value was augmented to 2000 [W/m.K] above 2273K. The electrodes are subjected to Joule heating during normal operations and to facilitate this in the model, the thermal conductivity value (k) of the electrodes in Table 1 was increased from 23 to 3000. This also prevented sub-cooling of the top part of the electrode.

RESULTS

The example represented here is the most up-to-date solved model at the time of publication and is a culmination of sensitivity analyses and parameter estimation performed on more than 70 previously solved CFD models. Four sets of results are summarised in Table 1. They represent sensitivity analyses results owing to changes in absorption and scattering coefficients (Model 2), the packed bed porosity (Model 3), energy input and feed flowrate (Model 4) as well as the reaction rate coefficient (Model 5). These models will be discussed later. Model 1 will now be discussed in-depth.

Reaction zone and P_2O_5 consumption

As shown by Dresen et al. (2002) and Van der Pas (1999), optimal reduction of phosphorus takes place in the solid-gas region (burden) of the furnace, with the liberated P_2O_5 gas having to diffuse from the reaction zone inside the pellet, migrate to the coke and then be reduced by the carbon (Mu, 1986). It is, therefore, important to understand the characteristics and optimise the behaviour of the gas-solid, main reaction zone (reductive blanket) within the feed burden. Figure 3 shows a thin reaction zone and a decrease in P_2O_5 concentration from 29.1 wt% to 4.7 wt%. This amounts to a 1.31 wt% P_2O_5 in the slag, which corresponds well to industry values (Table 1). In this ongoing study, one of the top priorities will continue to be the investigation of selected changes in a variety of variables on this reaction zone, as well as the conditions conducive to the maximisation thereof. This will facilitate in the understanding and eventual minimisation of the varying energy consumption created by complex feed materials (see Introduction).

Temperature

Figure 4 shows the temperature inside the furnace. The domed-area around the inlet volume (as depicted by the double-sided arrows) depicts the onset of gaseous product formation. Although not shown here due to the 1700 K visual display limit, the average temperature in the inlet volumes (indicated with the thick white and black arrow) is 2600 K. The colder areas indicated with the two elipses are where cold, fresh feed at a temperature of 573 K (for Model 1) is artificially introduced to the model.

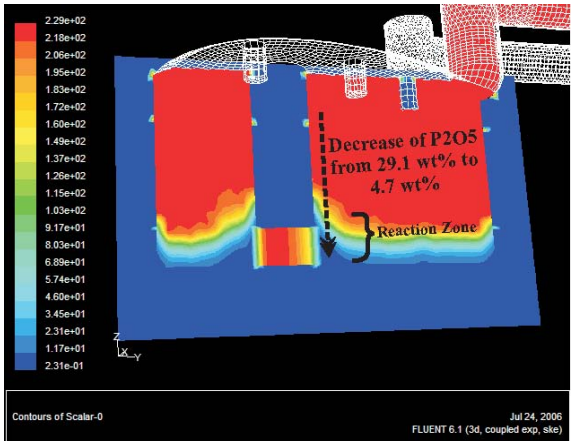

Figure 3: A cross-section of the P_2O_5 concentration (user-defined scalar) as it is consumed as part of the gaseous product reaction.

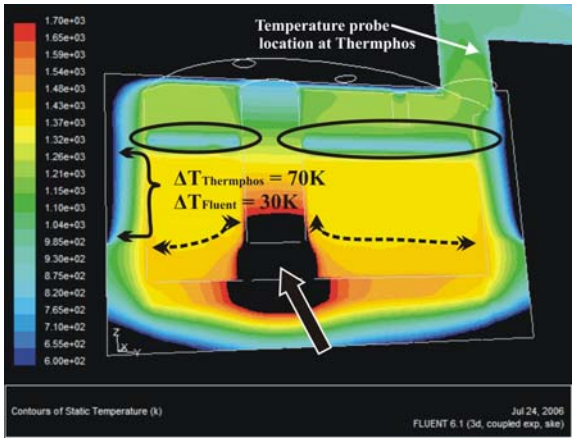

Figure 4: A cross-section of the temperature of the furnace. Note that one of the electrodes is also depicted in this picture.

Gaseous product formation and pressure drop

Figure 5 shows a two-dimensional view of the gaseous product flow vectors from one of the outlet ducts, as well as the velocity contours of the outlet ducts. This view provides insight into the causes of high gaseous outlet pressures that sporadically occur at Thermphos: Low, recirculating gaseous flow velocity areas causes dust accumulation and clogging, thus resulting in increased pressure. The furnace under investigation at Thermphos produced ≈3.10 [kg/s] of gas and the model flowrate value of 3.28 [kg/s] (1.64 kg/s per pipe) corresponds to within 6%. No constraints are put on this value when solving the model because it is essential for validation purposes and generated entirely as a dependent variable. The model showed a 45 [Pascal] pressure drop inside the packed bed.

Powerfactor

The most significant parameter at Thermphos is the powerfactor [MW/tonP_4]. It provides the best assessment of process efficiency and profitability. For the data investigated, Thermphos achieved a powerfactor of 30 [StandMW/tonP_4] (*This is not the actual value, but a standardized value*). For the solved models, the powerfactor is calculated from the sum of the energy sinks in Table 2 (numbers 2 → 9), divided by the P_4-gas production (number 13). The Model 1 powerfactor of 30.95 corresponds to within 0.4% of the Thermphos value. It is once again important to note here that no constraints were put on the variables required for the calculation of the powerfactor while solving the CFD model. The next section will briefly review Models 2 – 5.

Summary of results from Model 2 to Model 5

For Model 2, s = 0.5 and a = 0.5. This caused the temperature within the burden to drop and letting 20.5% of the P_2O_5 (amounting to 6.65 wt% P_2O_5 in the slag) enter the slag layer. Less gaseous product was produced and given the connection between gaseous product flowrate (2.81 kg/s) and Energy Sink - Reaction (29%) (Scheepers, Adema, Yang & Reuter, 2006), these values were too low, which also lowered the average gaseous outlet temperature (935K).
For Model 3, the porosity was changed to 32.0%. With the feed flowrate remaining unchanged, the residence time inside the furnace decreased. This provided less time for reaction (further from thermodynamic equilibrium) and this is again reflected (when compared to Model 1) in the decrease in the Energy Sink - Reaction value (35.3%) and the P_2O_5 content in the slag (2.78 wt%).
For Model 4, the parameters were deliberately chosen NOT to reflect reality to proof the model functionality outside realistic data. The Energy Input (93.3%) was decreased by 6.7%. The feed flowrate (10.65 kg/s), on the other hand, was also increased by 5\%, while in reality the feed flowrate will always decrease given its $R^2 = 0.88$ correlation with energy input for the data under investigation. This resulted in a residence time not long enough (5.91 hours) for the given energy input to produce the required gaseous product. This can again be seen in the high P_2O_5 content in the slag (6.36 wt%) and the exceptionally high and unprofitable powerfactor.
For Model 5, the feed flowrate (9.46 kg/s) was decreased to a value matching the lowered energy input (93.3%). This increased the residence time (7.69 hours) in the furnace. Along with this, the reaction rate was decreased (by changing the Reaction Rate coefficient). This provided enough time in the furnace for less Energy Input (93.3\%) to produce almost as much gaseous product (3.12 kg/s) as seen in Model 1. For this reason the powerfactor is the lowest of all the models, but the subsequent increase in the average gaseous outlet temperature (1100K) will, in reality, damage the downstream, electrostatic precipitators. Model 5 was the only example where the residence time was long enough to achieved conditions close to thermodynamic equilibrium. The next section will deal with additional validation techniques.

Additional model validation

As part of scheduled maintenance (performed in 2004) of a furnace at Thermphos, eight temperature probes were installed inside the carbon lining at a depth of 300mm from the outside and a height of 1650mm from the bottom of the furnace. Another five were installed vertically with an interval of 880mm between them.

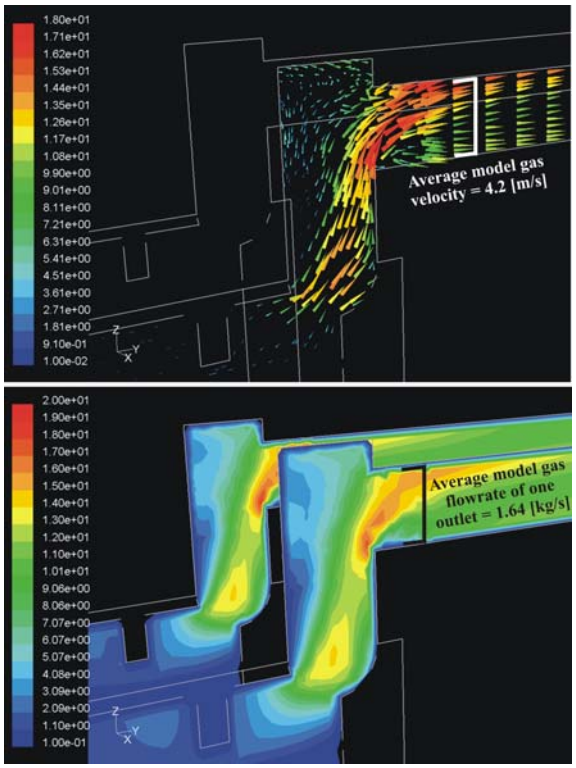

Figure 5: Top: Velocity vectors of the gaseous product for one of the outlets. Bottom: Velocity contours of the gaseous product for both of the outlets.

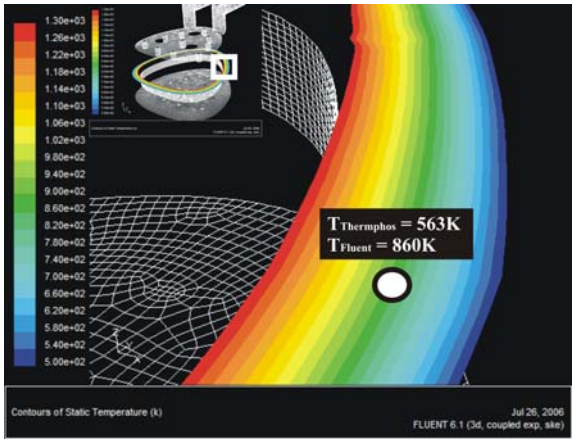

Figure 6: A close-up view of the temperature gradient inside the carbon lining at the height of 1650mm, with a comparison between actual Thermphos temperature values vs. model temperature values (Standard deviation on Thermphos value = ±70K).

Figure 6 shows the actual, average temperature value of the indicated probe at Thermphos to be 563K (Standard deviation on Thermphos value = ±70K). The difference could indicate that the thermal conductivity (7.5 W/m.K) value provided by the manufacturer for the actual carbon blocks in Table 1 might be too low. Figure 4 depicts the temperature difference in the top and bottom, vertically-installed, temperatures probes in the chamotte lining adjacent to the packed bed domain. A temperature gradient of 30K corresponds reasonably well with the average gradient value of 70K at Thermphos (Standard deviation on Thermphos value = ± 35K). By initialising the solver and setting up the boundary conditions with industrially verified results, parameter fitting is also guided within the constraints of these thirteen temperature probe values.

CONCLUDING REMARKS

P_2O_5 consumption results in Figure 3 reveal a narrow gas-solid, reaction zone where conditions are optimum for maximum phosphorus recovery. By identifying the significant operational variables and, more importantly, the influence of changes to these variables on this reaction zone, more knowledge is being acquired as to how the furnace can be controlled with the goal of maximising this volume and minimising the energy consumption.

Gaseous product and velocity information in Figure 5 shows low, recirculating gaseous flow velocity areas that cause dust accumulation, thus resulting in increased pressure measurement in the outlet duct. This is a common problem at Thermphos now being confronted in a more knowledgeable way.

This model has potential to validate or even determining the (often unknown) reaction rate information of new feed material or vice versa, what process conditions could be expected if the reaction rates are known.

This paper (in part) provides an in-depth, case-specific CFD model catering to the exact needs of the submerged arc furnace, phosphorous producers. The exceptional agreement between actual and theoretical powerfactors shows that this model provides real, industrial answer to real, industrial problems and scenarios.

The integration of accurate, multi-field thermodynamical data (Factsage 5.4.1, 2006) with computational flow dynamics (Fluent 6.1.18, 2003) has proved to be successful, further unifying the sciences of kinetics and equilibrium thermodynamics.

As additional information like mineralogy analysis of dig-out samples for temperature validation becomes available (in progress) these new mathematical models can be implemented in order to improve, not only accuracy of CFD model, but also the Dynamic-CFD hybrid control model as a whole.

Future work includes investigating various electrode heights and the unsymmetrical energy inputs that occurs as a result thereof, as well as optimising the model further to minimise the consistently negative energy balance and slightly elevated gaseous outlet temperature (Table 1). It is also planned to re-define the bottom cooling flux to eliminate over cooling of the carbon brick domain, to continue the sensitivity analysis and parameter estimation already in progress and to compensate for freeze-lining.

Submerged arc furnaces normally have long time periods between sampling and very complex metallurgy, but it is believed that this Dynamic-CFD hybrid-based predictive strategy will ultimately provide strong, on-line indications of the dynamic path of the process.

ACKNOWLEDGEMENTS

The authors would like to thank Thermphos and Senter-Novem for their interest and financial support in this ongoing study.

REFERENCES

CORBRIDGE, D., (1995), "Phosphorus: An outline of its chemistry, biochemistry and uses", **5th**, Amsterdam.

DRESEN, C., VONCKEN, J., SCHIPPER, W., DE RUITER, R. and REUTER, M.A., (2002), "Optimisation of pellet production in a phosphorous furnace", *TMS Annual Meeting,* Extraction and Processing Division, 435-448.

FACTSAGE 5.4.1 (2006), www.factsage.com

FLUENT 6.1.18 (200), www.fluent.com

GAMBIT 2.04 (2006), www.fluent.com

GU, L. and IRONS, G., (1998), "Physical and mathematical modelling of fluid flow in electric arc furnaces", *Electrical Furnace Conference Proceedings,* Vol.56, Iron and Steel Society, 411-420.

INCROPERA, F. and DE WITT, D., (1990), Fundamentals of Heat and Mass Transfer, **3rd**, John Willey and Sons.

MU, J., LEDER, F., PARK, W., HARD, R., MEGY, J. and REISS, H., (1986), "Reduction of phosphate ore by carbon: Part 2. Rate limiting steps", *Metallurgical Transactions B,* **17B**, 869-877.

ROBIETTE, A. and ALLEN, A., (1972), Electric Melting Practice, London.

SCHEEPERS, E., YANG, Y., ADEMA, A.T. and REUTER, M.A., (2006), "A Dynamic-CFD hybrid model of a submerged arc furnace for phosphorous production", *Minerals Engineering,* **19**(3), 309-317.

SCHEEPERS, E., ADEMA, A.T., YANG, Y. and REUTER, M.A., (2006), "The development of a CFD model of a submerged arc furnace for phosphorous production", *Minerals Engineering,* In press, Accepted: 8 May 2006.

ULLMANN'S Encyclopedia of Industrial Chemistry, (2000), Electronic Release, **6th**.

VAN DER PAS, D., (1999), "Kinetiekstudie betreffende de reduction van fosfaaterts", *Master's Thesis,* Delft University of Technology, The Netherlands.

APPENDIX

Solved model results.

		Thermphos data under investigation
1	**Energy Input (arcs)**	**100%**
2	Cooling – Bottom	
3	Cooling – Side	
4	Cooling – Exposed furnace	
5	Cooling – Electrodes	
6	Cooling – Outlet pipe wall	
7	Heat loss – gaseous product	
8	**Energy sink – Reaction**	≈ **53%** (Ullmann's)
9	**Energy sink – Heating/Melting**	≈ **31%** (Ullmann's)
10	**ENERGY BALANCE**	
11	Feed flowrate [kg/s]	10.15(±0.5)
12	Gaseous product flowrate [kg/s]	≈ 3.1
13	P_4 flowrate [kg/s]	≈ 0.83
14	**P_2O_5 wt% in the slag**	**1.5((±38%)**
15	**POWERFACTOR**	**30**
16	Slag T [K]	1723(±50K)
17	Onset T of gaseous reaction [K]	1473
18	Inlet zone T [K]	N/A
19	Gaseous outlet T [K]	728(±25K)
20	Pressure drop in packed bed [K]	Varying
21	Residence time in furnace [hours]	7.2(±0.2)
22	Downward burden speed [m/s]	$1.48e^{-4}$
23	Packed bed porosity [kg/m^3]	37.7%
24	Reaction rate coefficient [1/s]	Varying
25	Scattering coefficient	N/A
26	Absorption coefficient	N/A
27	Number of iterations	N/A
28	Radiation model	N/A
29	T of new feed material [K]	N/A
30	Initialised scalar (P_2O_5) [kg/m^3]	Varying

Table 2a: A summary of input and boundary conditions, as well as solved model results. The underlined values refer to the parameters pre-fixed by the user, while the other values were calculated by Fluent 6.1.18 (2003) and used as validation. The underlined values associated with Models 2 - 5 reflect the parameters changed for that particular solved model - thus performing a sensitivity analysis on selected variables. If not shown, the underlined values associated with Model 1 apply to Models 2 - 5.

	Model 1	Model 2	Model 3	Model 4	Model 5
1	100%			93.3%	93.3%
2	2.7%				
3	0.7%				
4	0.75%	0.78%	0.75%	0.71%	0.84%
5	11.1%				
6	3.3%	3.2%	3.3%	2.7%	4.4%
7	5.6%	5.1%	5.8%	6.3%	8.1%
8	**40.3%**	**29%**	**35.3%**	**39.4%**	**30.6%**
9	**32.4%**	**33.1%**	**31.9%**	**27.3%**	**33.6%**
10	**-3.2%**	**-14.3%**	**-8.4%**	**-8.1%**	**-6.9%**
11	10.15			10.65	9.46
12	3.28	2.81	3.24	2.06	3.12
13	0.87	0.726	0.858	0.494	0.819
14	**1.31**	**6.65**	**2.78**	**6.36**	**0.37**
15	**30.95**	**32.8**	**29.7**	**48.2**	**29.2**
16	1600	1596	1610	1826	1526
17	1423				
18	2600	2583	2556	2395	2378
19	970	935	944	892	1101
20	45	59	56	74	94
21	7.18		6.75	5.91	7.69
22	$1.48e^{-4}$		$1.37e^{-4}$	$1.55e^{-4}$	$1.38e^{-4}$
23	37.7%		32.0%		
24	0.0003T – 0.40				0.0003T – 0.41
25	0.9	0.5			
26	0.9	0.5			
27	5500	25000			
28	P1				
29	573	773	773	773	773
30	229		250		

Table 2b: Refer to Table 2a.